Characterization of Polystyrene Conformation by Solid-State NMR Correlation of C−^{2}H and ^{13}C−^{13}C Bond Orientations

M. G. Dunbar, D. Sandström,† and K. Schmidt-Rohr*

Department of Polymer Science and Engineering, University of Massachusetts at Amherst, Amherst, Massachusetts 01003

Received December 13, 1999; Revised Manuscript Received May 25, 2000

ABSTRACT: The backbone conformation of polystyrene (PS) is investigated by two-dimensional solid-state NMR. The experiment correlates well-defined nuclear spin interactions, the ^{13}C−^{13}C dipolar coupling along a backbone bond, and the ^{2}H quadrupolar coupling along the C−^{2}H bond in an adjacent repeat unit of a suitably isotopically labeled PS. The pulse sequence is based on a heteronuclear multiple-quantum coherence (HMQC) approach. In addition, ^{13}C−^{13}C dipolar decoupling is applied during excitation and reconversion of the heteronuclear coherences, and the ^{13}C−^{13}C dipolar coupling is detected. The two-dimensional spectral patterns obtained for gauche-bar ($\bar{g}$) conformations are clearly distinct from the gauche (g) and trans (t) patterns. The fraction of the $\bar{g}$ conformation is found to be too low to be detected in the experimental spectrum. The patterns are highly sensitive to the torsion angle near trans. The maximum in the torsion angle distribution in PS is found to be centered at 180°, within ±10°. This contradicts the predictions of an atomistic model of PS. The trans peak is relatively narrow (standard deviation < 30°), indicating that the rotational-isomeric-state approximation is quite suitable.

Introduction

Two-dimensional solid-state nuclear magnetic resonance (NMR) provides some of the best available techniques for characterizing the backbone torsion angles in amorphous solid polymers.[1−4] So far, most of such NMR investigations have involved chemical shift anisotropies (CSAs). For instance, double-quantum correlation of the CSAs of CH_2 groups in neighboring segments of polystyrene (PS) has revealed ∼68% trans conformations.[3] However, due to uncertainties of the chemical shift tensor orientation, the width of the maxima in the torsion angle distribution could not be determined with sufficient precision. In addition, g and $\bar{g}$ conformations could not be distinguished, for symmetry reasons.

In this paper, we introduce a two-dimensional (2D) NMR experiment to obtain information on polymer backbone conformations based on well-defined interactions that are oriented along specific bonds. This is achieved by correlation of the ^{2}H quadrupolar coupling, which probes the C−^{2}H bond direction, with the ^{13}C−^{13}C dipolar coupling, which is directed along the backbone bond of an adjacent segment. The symmetry of these interactions is such that $\bar{g}$ conformations give different spectral patterns than g and t conformations; the latter two, however, produce similar features. Because of the reliable orientation of the principal axes of the NMR interaction tensors along specific bond directions, the position and width of the dominant trans maximum in polystyrene can be determined. The sample used is a random copolymer of 10% [α+β-^{13}C]styrene and 90% [α-^{2}H]styrene.

† On leave from the Division of Physical Chemistry, Arrhenius Laboratory, Stockholm University, Sweden.

* To whom correspondence should be addressed at: Department of Chemistry, Iowa State University, Ames, IA 50011. E-mail: srohr@iastate.edu.

Experimental Section

Sample Preparation. Poly([α+β-^{13}C]styrene-*co*-[α-^{2}H]styrene): Unless otherwise noted, materials were obtained from commercial suppliers and used without further purification. The [α-^{2}H]styrene (Cambridge Isotope) and [α+β-^{13}C]styrene (Isotech) were inhibited with 10 ppm 4-*tert*-butylcatechol. To a 20 mL ampule containing a stirbar was added [α-^{2}H]styrene (0.9 mL) and [α+β-^{13}C]styrene (0.10 mL). Benzene (0.4 mL) and 0.4% AIBN (2,2′-azoisobutyronitrile) (w/w) in benzene (0.4 mL) were added to the 20 mL ampule with a syringe. The mixture was then subject to freeze/pump/thaw cycles three times to remove any dissolved gases. Still under vacuum, the mixture was placed into a 65 °C temperature bath for 24 h. The resulting poly([α+β-^{13}C]styrene-*co*-[α-^{2}H]styrene) was dissolved in 10 mL of benzene and then filtered. The filtered solution was precipitated in 300 mL of methanol, filtered, and washed with 100 mL of methanol. The white polystyrene was dried under vacuum.

The ^{13}C labeling level of 10% provides a sufficiently strong ^{13}C signal but also ensures a sufficiently large typical distance between ^{13}C's in different segments. Because of the 90% deuteration, most ^{13}C−^{13}C pairs are only two bonds from a deuteron, so that the ^{13}C−^{2}H transfer is relatively efficient.

NMR. The NMR experiments were performed at a field of 7.0 T on a Bruker DSX300 spectrometer using a 4 mm triple-resonance MAS probehead, but without sample rotation. Typical radio-frequency field strengths $\gamma B_1/2\pi$ were 105 kHz for ^{1}H decoupling, 60 kHz for ^{13}C, and 90 kHz for ^{2}H. The best signal was obtained with ^{2}H pulses of 2 μs, which is shorter than the 90° pulse length of 2.9 μs. A ^{1}H−^{13}C cross-polarization (CP) time of 0.5 ms and a heteronuclear-coherence excitation period of 1.75 ms were used. Twenty-four time-data points in t_1 were acquired with increments of 2 μs. For each t_1 point, 512 scans were averaged. The total time for the spectrum of Figure 5a was 50 h.

Theory

In this section, we discuss the NMR pulse sequence and the related requirements of decoupling of various interactions and the dependence of the two-dimensional spectral patterns on the torsion angle.

10.1021/ma992083d CCC: $19.00
Published on Web 07/21/2000

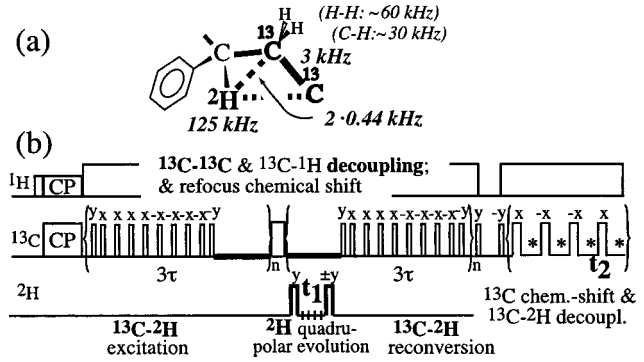

Figure 1. (a) Nuclear spin interactions relevant in the isotopically labeled polystyrene used. (b) Pulse sequence for correlating the ^{2}H quadrupolar coupling in t_1/ω_1 with the pure ^{13}C−^{13}C dipolar coupling in t_2/ω_2.

Pulse Sequence. The ^{2}H/^{13}C−^{13}C correlation experiment, with the pulse sequence of Figure 1, correlates the ^{2}H quadrupolar interaction in the ω_1 dimension of the 2D spectrum with the ^{13}C−^{13}C dipolar coupling in ω_2. The resulting spectral pattern provides information on the relative orientation of the ^{13}C−^{13}C and C−^{2}H bonds.

Figure 1a schematically shows parts of two PS repeat units: one containing a C−^{2}H group and the other a ^{13}C−^{13}C pair in the backbone. A large number of NMR spin couplings must be considered in this system. In addition to the ^{2}H−^{13}C, ^{1}H−^{13}C, and ^{1}H−^{1}H dipolar couplings and the ^{2}H quadrupolar coupling indicated in Figure 1a, the ^{13}C chemical shift interaction must also be taken into account.

The product-operator treatment of the ^{2}H−^{13}C heteronuclear multiple-quantum coherence (HMQC) experiment is different from that of the usual spin-$^1/_2$ HMQC since ^{2}H is a spin-1 nucleus; it is described, for instance, in ref 5. Nevertheless, the same heteronuclear coherence S_x L_x is central in this experiment. To generate this heteronuclear coherence, the heteronuclear dipolar coupling must act undisturbed on transverse ^{13}C magnetization or coherence. Therefore, the 2 orders of magnitude stronger ^{2}H quadrupolar coupling must be removed. In the pulse sequence of Figure 1b, this is achieved simply by ensuring that the ^{2}H component of the coherence remains along the *z*-direction, so that it commutes with and therefore remains unaffected by the quadrupolar interaction.

The decoupling of the ^{13}C−^{13}C dipolar coupling is more challenging. Of several possible multiple-pulse decoupling methods, we chose a "complete decoupling" scheme using a magic-sandwich-echo derived sequence with a basic 10-pulse cycle[6] combined with strong heteronuclear decoupling. Its parameters can be optimized using a pulse sequence closely resembling that of Figure 1b, only with the ^{2}H pulses removed and the receiver phase correspondingly altered: delays and pulse lengths are optimized near their theoretical values to retain the outer parts of the ^{13}C−^{13}C dipolar Pake powder pattern observed after application of the multiple-pulse sequence. During the t_1 period, the strong quadrupolar coupling dominates the evolution of the coherence. Still, the evolution period is placed into the large window of one cycle of the "complete-decoupling" sequence to minimize ^{13}C−^{13}C dipolar effects for long evolution times t_1. This is possible since the longest ^{2}H evolution time necessary is shorter than the window length of 34 μs. A ^{13}C 180° pulse at the center of the heteronuclear-coherence excitation and reconversion period refocuses the ^{13}C chemical shift. During detection, to observe the pure ^{13}C−^{13}C dipolar coupling, the ^{13}C chemical shift and the ^{13}C−^{2}H dipolar coupling are refocused by a series of 180° pulses on the ^{13}C channel; the magnetization is detected in the center of the 50 μs windows between the pulses.

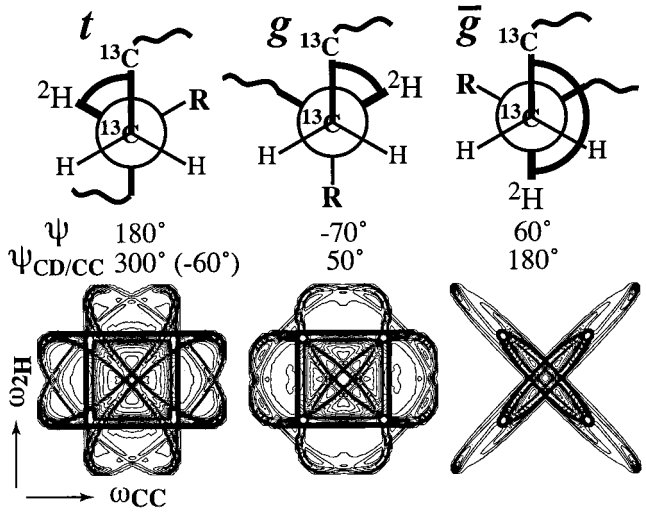

Figure 2. Distinction between t/g and ḡ conformations, and examples of ^{2}H/^{13}C−^{13}C correlation patterns. Top: Newman projections, showing that t and g conformations have similar C−C−C−^{2}H torsion angles ($\psi_{CD/CC}$) of ~60°, while ḡ has a ~180° C−C−C−^{2}H torsion angle ($\psi_{CD/CC}$). The two-dimensional spectral patterns shown at the bottom reflect the fact that the ^{13}C−^{13}C and C−^{2}H bonds are nearly parallel in the ḡ conformation, very different from the g and t conformation.

The ^{13}C T_2 (spin−spin) relaxation in 15% $^{13}CH_2$-labeled polystyrene measured under 7 kHz magic-angle spinning is well described by $\exp(-(t/\ 8\ \text{ms})^{0.8})$; thus, on the 2 ms time scale of the experiment described here, differential relaxation of specific conformations will be insignificant.

Torsion Angle Dependence of 2D Patterns. Figure 2 shows examples of ^{2}H−^{13}C NMR correlation patterns for t, g, and ḡ conformations as defined by the Newman projections at the top. Because of the symmetry of the one-dimensional dipolar and quadrupolar patterns, the two-dimensional patterns are symmetric in both dimensions. This means that the same spectral pattern, shaded gray for the trans conformation in Figure 2, repeats $2 \times 2 = 4$ times in the spectrum. Since the various "copies" overlap, the clarity of the spectrum is reduced compared to a "single-transition" spectrum as obtained when chemical shift anisotropies are correlated.[6]

Figure 3a displays a series of ^{2}H−^{13}C correlation spectra for various torsion angles. The top row represents patterns for conformations near ḡ, the second row spectra for torsion angles near t or g, and the third some examples for torsion angles between t and g. In Figure 3b, the spectrum for random relative orientations of C−^{2}H and ^{13}C−^{13}C bonds is shown. It was generated as the product of the ^{2}H and ^{13}C powder spectra, but for one "transition" only, and the resulting pattern was reflected at $\omega_1 = 0$ and $\omega_2 = 0$ to generate all four subspectra, which were added up. Note that it is not the sum of the spectra for all torsion angles ψ, since these represent rotations around only one axis.

The quantity measured directly by the spectral line shape is $\beta_{CD/CC}$, the angle between the C−^{2}H and the

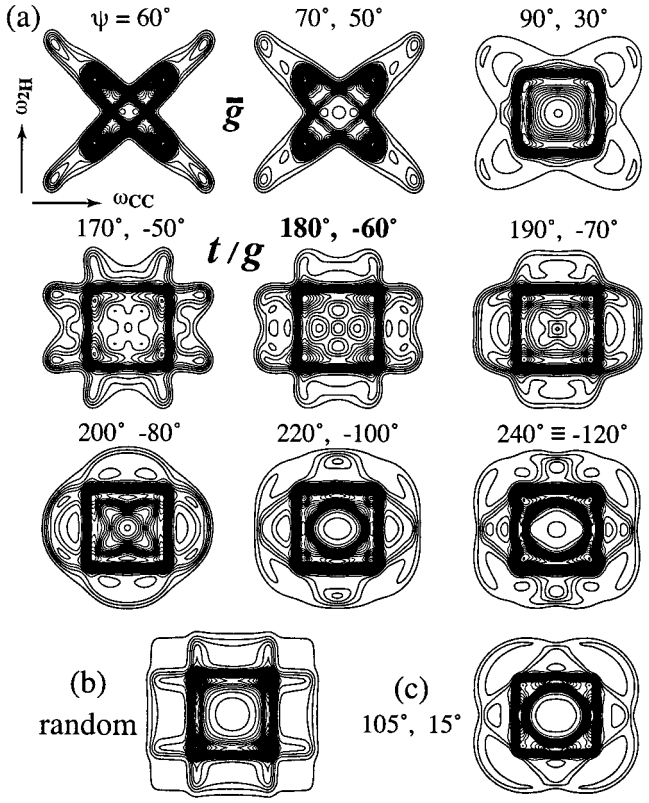

Figure 3. (a) Series of $^2H/^{13}C-^{13}C$ correlation patterns as a function of torsion angles, with a heteronuclear-coherence excitation time of 1.75 ms. The line broadenings applied to the spectra are comparable to those of the experimental spectrum shown in Figure 5a. The angles in the top row are close to $\bar{g}$; those in the second row are close to t and g; the patterns in the third row show that near $\psi = 240°$ or 120° the angular resolution is much lower than near 180° and 60°. (b) Spectrum for random distribution of relative orientations of the $C-^2H$ and $^{13}C-^{13}C$ bonds. (c) Spectrum with $\psi = 105°$ or 15°. It has the same $\beta_{CD/CC}{}^r$ value of 42° as the spectrum directly above it ($\psi = 240°$ or $-120°$), but with a different $\beta_{CD/CC}$ value. Because of different double-quantum excitation factors, the spectra are not identical, and the torsion angles of $\psi = 105°$ and 240° can be distinguished to some extent.

$^{13}C-^{13}C$ bond directions. As is well-known from ^2H NMR, the fundamental 2D powder pattern for uniaxial interactions consists of an elliptical ridge and two straight "90° ridges" connecting the ellipse with one corner of the spectrum.[7,8] The shape of the elliptical ridge pattern is related to $\beta_{CD/CC}$ according to

$$\tan(\beta_{CD/CC}) = |b/a| \quad (1)$$

where b and a are the half-axes of the ellipse.[7,8] Here, it is assumed that the anisotropy parameters δ in both dimensions are scaled to the same length in the plot.

The angle $\beta_{CD/CC}$ depends on the dihedral angle $\psi_{CD/CC}$ (the angle between the projections of the $C-^2H$ and $^{13}C-^{13}C$ bonds), on the $C-^{13}C-^{13}C$ bond angle θ_{CCC}, and on the $^2H-C-^{13}C$ bond angle θ_{DCC} (see Figure 4a). The relation is

$$\cos(\beta_{CD/CC}) = \cos(\theta_{DCC})\cos(\theta_{CCC}) - \sin(\theta_{DCC})\sin(\theta_{CCC})\cos(\psi_{CD/CC}) \quad (2)$$

according to the cosine theorem of spherical trigonometry, which is easily derived by calculating the dot product between the $C-^2H$ and $^{13}C-^{13}C$ direction

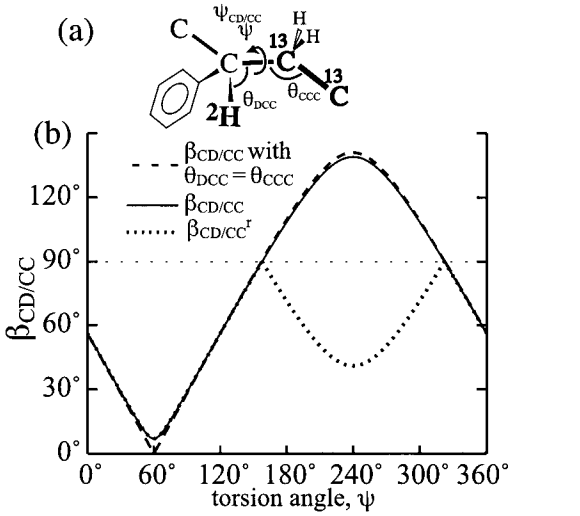

Figure 4. (a) Definition of angles relevant in the torsion angle measurement. The bond angles θ_{CCC} and θ_{DCC} are defined by $C-^{13}C-^{13}C$ and $^2H-C-^{13}C$ bonds, respectively. The torsion angles $\psi_{CD/CC}$ and ψ are defined by $^2H-C-^{13}C-^{13}C$ and $C-C-^{13}C-^{13}C$ bonds, respectively. (b) Dependence of the angle $\beta_{CD/CC}$ and $\beta_{CD/CC}{}^r$ on the torsion angle ψ. The dashed line, which reaches $\beta_{CD/CC} = 0$, shows the dependence of $\beta_{CD/CC}{}^r$ on ψ when $\theta_{CCC} = \theta_{DCC} = 109.5°$. The calculations for the two other lines used more realistic bond angles of $\theta_{CCC} = 114°$ and $\theta_{DCC} = 107°$. The solid line is the plot of $\beta_{CD/CC}$ according to eq 2, while the dotted line with the second minimum at 240° shows the dependence of $\beta_{CD/CC}{}^r$ (eq 4) on ψ. The vanishing slope of these curves near $\psi = 240°$ indicates a weak angle dependence (low torsion-angle resolution) in that range.

expressed in polar coordinates in a system where the $C-^{13}C$ axis is the z-axis (the first C refers to the carbon bonded to the deuteron).

To obtain the relevant dependence on the conventional torsion angle ψ, we note that

$$\psi_{CD/CC} = \psi + 120° \quad \text{or} \quad \psi = \psi_{CD/CC} - 120° = \psi_{CD/CC} + 240° \quad (3)$$

which can be quite easily verified on the Newman projections of Figure 2. Combining eqs 2 and 3, the angle $\beta_{CD/CC}$ is plotted in Figure 4b as a function of the torsion angle ψ. The dashed line shows the dependence obtained if perfectly tetrahedral $C-^{13}C-^{13}C$ and $^2H-C-^{13}C$ bond angles are assumed; the full line is the case of more realistic bond angles of $\theta_{CCC} = 114°$ and $\theta_{DCC} = 107°$.[9]

According to eq 1, spectra for $\pm\psi_{CD/CC}$ are identical, since $\cos(\psi_{CD/CC}) = \cos(-\psi_{CD/CC})$. Inserting this into eq 2, we conclude that for angle pairs $\psi_\pm = 240° \pm \Delta\psi$, e.g., for 220° and 260°, or equivalently for $\psi_\pm = 60° \pm \Delta\psi$, the same spectra are observed. This is confirmed by equal $\beta_{CD/CC}$ values for these torsion angle pairs (see Figure 4b).

Normally, NMR measurements cannot determine the polarity of the internuclear vectors, and therefore $\beta_{CD/CC} = \beta$ and $\beta_{CD/CC}{}' = 180° - \beta$ should give the same spectrum. A variant $\beta_{CD/CC}{}^r$ of $\beta_{CD/CC}$ that is suitably restricted to $0° \le \beta_{CD/CC}{}^r \le 90°$ (see dashed line in Figure 4b) can be obtained from

$$\cos(\beta_{CD/CC}{}^r) = |\cos(\theta_{DCC})\cos(\theta_{CCC}) - \sin(\theta_{DCC})\sin(\theta_{CCC})\cos(\psi_{CD/CC})| \quad (4)$$

However, the excitation factor of the $^2H-^{13}C$ coherence can break this symmetry. Therefore, two torsion angles

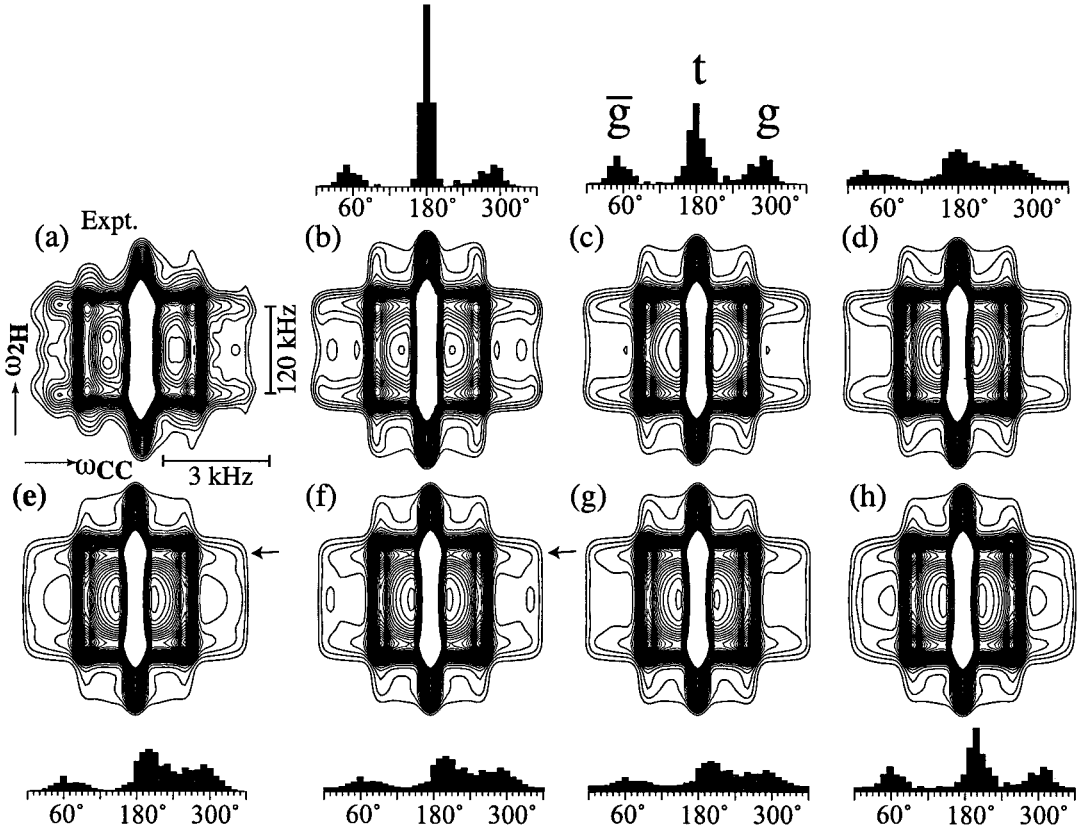

Figure 5. $^2H/^{13}C-^{13}C$ correlation patterns of poly([α+β-^{13}C]styrene-*co*-[α-^{2}H]styrene). For the simulations, the distribution of torsion angles used is shown above or below each simulated spectrum. (a) Experimental spectrum. (b) Best simulation found, based on a RIS model with ±8° wide trans peak centered at 180°; the remainder of the torsion angle distribution is the same as in (c). (c) Simulation with ±15° wide trans peak centered at 180°, according to ref 17. (d) Simulation with ±30° wide trans peak centered at 180°, with 25% of a random-orientation spectrum added. (e) Simulation with ±30° wide trans peak centered near 200° according to ref 13. The arrow points at a ridge that is significantly too low, compared with the experimental spectrum in (a). (f) Same as (e), but with 25% of a random-orientation spectrum added. (g) Same as (e), but with 40% of a random-orientation spectrum added. (h) Simulation with ±15° wide peaks, with trans centered at 200°, and 25% of a random-orientation spectrum added. The random-orientation contribution is plotted as a constant across the torsion angle distribution.

ψ and ψ' with $\beta_{CD/CC}{}^r(\psi) = \beta_{CD/CC}{}^r(\psi')$ but $\beta_{CD/CC}(\psi) \neq \beta_{CD/CC}(\psi')$ have similar but not equal spectral patterns. An example is shown in Figure 3, where the outlines of the pattern shown in (c), with $\beta_{CD/CC}{}^r(105°) = 42°$ and $\beta_{CD/CC}(105°) = 42°$, match those for the pattern right above it for $\psi = 240°$, which has the same $\beta_{CD/CC}{}^r(240°) = 42°$; however, details of the intensity distribution are different because $\beta_{CD/CC}(240°) = 139°$ is not the same as for the pattern in (c).

Spectral Patterns for t, g, and ḡ. The top row of Figure 2 shows the Newman projections of the trans (t), gauche (g), and gauche-bar (ḡ) states.[9−11] In the ḡ conformation, the bulky side group and chain continuations are all on one side. Correspondingly, the ḡ state is always less populated than the g state. In the RIS model of Flory and Fujiwara, the ḡ state is completely absent. [9]

As shown in Figure 2, the symmetry of the interactions probed is such that t and g conformations have nearly equivalent $\psi_{CD/CC}$ dihedral angles of $\psi_{CD/CC} \approx \pm 60°$, while ḡ has a distinct $\psi_{CD/CC} \approx 180°$. If the bond angles in PS were all exactly tetrahedral, the exact $\psi_{CD/CC} = 180°$ ḡ pattern would consist of a cross of two perfectly straight ridges, along the diagonal and anti-diagonal. This can be easily understood from the fact that this would lead to the $^{13}C-^{13}C$ and $C-^2H$ bonds being exactly parallel. Mathematically, eq 2 for $\psi_{CD/CC} = 180°$ and $\theta_{DCC} = \theta_{CCC}$ (which is actually a weaker requirement than tetrahedral bond angles) yields $\beta_{CD/CC} = 0$. However, the simulations were performed with more realistic bond angles of $\theta_{DCC} = 107°$ and $\theta_{CCC} = 114°$, [9] which lead to nonparallel $C-^2H$ and $^{13}C-^{13}C$ bonds and spreading of the straight ridges into narrow ellipses, even for $\psi_{CD/CC} = 180°$.

Results and Discussion

Experimental 2D Pattern. Figure 5a shows the experimental $^2H/^{13}C-^{13}C$ correlation spectrum obtained for polystyrene. Comparison with the simulated spectra of Figure 3 clearly shows that the predominant torsion angles are near the t and g conformations. The deviations in the outer regions of the experimental spectrum in ω_1, where the quadrupolar coupling is larger than the B_1 field, are expected; the low outer shoulders in ^2H quadrupolar spectra are notoriously poorly excited.[12] The effect of the dead time induced by the finite ^2H frequency pulse width, which manifests itself most prominently in a suppression of the broad center of the ^2H spectrum with respect to the peaks, was reduced by back-extrapolation of the time data by half a dwell time (i.e., 1 μs) in t_1.

The experimental pattern contains an intense vertical ridge in the center (at $\omega_2 = 0$), due to naturally occurring isolated ^{13}C. Given that only two out of eight carbons are labeled in 10% of the repeat units, the ^{13}C nuclei in natural abundance make up $8 \times 0.9 \times 0.011/(2 \times 0.1)$

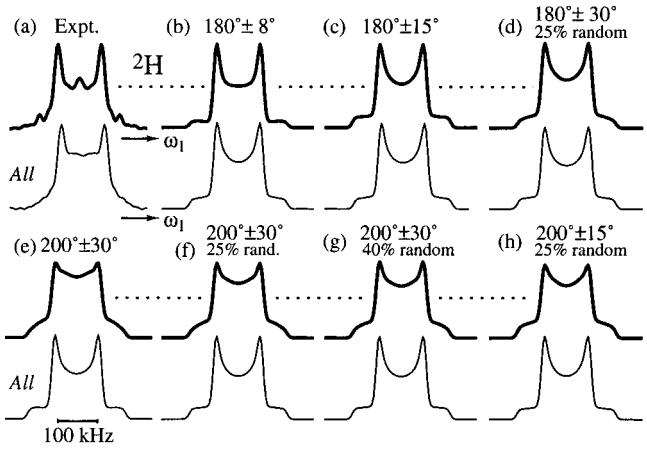

Figure 6. One-dimensional ^2H spectra obtained by adding the signals of the "ω_2-shoulders" of the spectra in Figure 5. Below each of these partial projections, the corresponding full projection onto the ω_1-axis is shown for reference. The parameters for (a)−(h) are the same as for the corresponding parts of Figure 5. The decreased intensity at the outermost shoulders in (a) is due to the well-known excitation problem in ^2H NMR, which arises because the B_1 field of the pulse is weaker than the strongest ^2H quadrupolar couplings.

= 40% of all ^{13}C's in the sample. In the spectrum, they account for 30−40% of the intensity. Their signal is so intense for several reasons: (i) its width in ω_2 is small; (ii) in $^{13}C-^2H$ groups, the coherence transfer is more efficient than in the two-bond case; and (iii) due to its weak $^{13}C-^{13}C$ dipolar coupling, it decays more slowly in the heteronuclear coherence excitation and reconversion periods. In principle, this ridge of the isolated spin pairs could be suppressed by a double-quantum filter,[3] but this would unacceptably reduce the signal-to-noise ratio.

Comparison with Models. Figure 5b−f shows spectra simulated on the basis of various torsion angle distributions. At first sight, the main features, for instance the dominant square of ridges in the center of each spectrum, are similar for all the spectra shown. This is not surprising, given that the t and g states dominate the torsion angle distribution in all the models used.

As the series of spectra in Figure 3 shows, the spectral region with the highest sensitivity to the torsion angle is that outside the central square. In this area, in particular on the left and right, significant differences between the simulations of Figure 5b−d can be observed. To facilitate comparison of the intensity distributions in these shoulders, their intensity distributions have been added up, and the resulting ^2H spectra are displayed in Figure 6. For reference, the nearly invariant integral projection of each full spectrum onto the ω_1 axis is shown below (thinner lines).

We have also measured the corresponding direct ^2H NMR spectrum of this sample to make sure that no motional distortions occur. Regular Pake powder patterns[12] with splittings of ∼120 kHz were obtained between 213 and 368 K; this excludes large-amplitude motions at room temperature. The splitting decreases slightly with increasing temperature, indicating small-angle (<5°) librations of the $C-^2H$ bonds. This angular amplitude is within our torsion angle error margins and therefore does not affect our results significantly.

The spectra in Figures 5b/6b and 5c/6c are in reasonable agreement with the experimental spectra of Figures 5a/6a. The model of Figures 5b/6b has a t content of 68% and a $\bar{g}$ fraction of 13%, which is essentially invisible at the contour levels shown (see discussion below). The peaks in the torsion angle distribution are relatively narrow, approximately ±8° (which corresponds to a full width at half-maximum of 19°). The model of Figures 5c/6c is that of ref 11, which exhibits peaks at 180° (56%), 300° (24%), and 60° (20%), with widths of approximately ±15°. The deviations from the experimental spectra of Figures 5a/6a are larger for the spectra in Figures 5d/6d, which were produced using trans and gauche peaks of ±30° widths.

Major differences are observed between the experimental spectra of Figure 5a/6a and the spectra of Figure 5e/6e, which are based on the atomistic simulation of ref 13. The horizontal ridges clearly observed near the left and right ends of the experimental spectrum are absent in the simulation. Instead, an arc pattern is observed in the 2D spectrum of Figure 5e, which is also recognized in the spectra of the third row of Figure 3, for angles between 200°/−80° and 240°; in the one-dimensional pattern of Figure 6e, this leads to a filling-in of the central part of the spectrum. Indeed, in the model of ref 13, the trans peak is shifted to 200°, and the 200°−280° (i.e., −80°) region between t and g is strongly populated, since the peaks have a width of ±30°. The shortcomings of this distribution, which are clearly shown here, have also been recognized in more recent work by Suter and co-workers, published after the initial submission of this paper.[14]

By unfortunate coincidence, the 2D pattern for the t (ψ = 180°) and g (ψ = −60°) conformations resembles that of random relative orientations of $C-^2H$ and $^{13}C-^{13}C$ bonds (Figure 3b). The random orientation spectrum must be taken into consideration, since a small fraction of more or less random long-range correlations is observed in many correlation spectra in amorphous materials.[15,16] To assess the potential effect of such a random background on the simulated spectra of Figure 5e/6e, 25% of the random component was added to 75% of the spectrum for the ±30° model. The resulting spectra, Figures 5f/6f, still show significant deviations from the experimental patterns. Only with 40% or more of a random component (Figures 5g/6g) does the ridge marked by an arrow in Figure 5f, and the corresponding "horn" in Figures 6f, become prominent enough to start matching that in the experimental spectrum. However, from comparison with similar $^2H-^{13}C$ correlation experiments on PAN,[15] where the trans−trans patterns are narrow (similar to the $\bar{g}$ patterns of Figures 2 and 3), so that the random background can be identified quite easily, it is known that such a random background accounts for less than 40% of the total intensity. For the 8° and 15° models (Figures 5b/6b and 5c/6c), addition of the random component actually decreases the quality of the fit to some extent. The difference between Figures 5a/6a and the simulation of Figures 5h/6h, with a ±15° peak at 200°, shows that a trans peak at 200°, even if it is narrow, can be ruled out.

Gauche-Bar Signal. In principle, the shape of the $\bar{g}$ pattern is very distinct (see Figures 2 and 3). However, neither in the experimental spectrum of Figure 5a nor in the simulations of Figure 5b−f is it observed specifically. A number of factors conspire to make the $\bar{g}$ signal hard to detect: (i) high angular sensitivity near $\bar{g}$ (see top row in Figure 3), which, given the wide (±20°) range of $\bar{g}$ angles in the models, spreads the signal out over a wide spectral area; (ii) the insufficient excitation of the

signal for the largest ^{2}H quadrupolar couplings, i.e., near the outer edges of the ^{2}H pattern, where the ḡ signals come together to form a (still broad) peak; (iii) dominance of the combined g and t patterns; (iv) possible "ditches" along the crossing diagonals (see 170° and 190° spectra in Figure 3) that cancel the ḡ signals in the central region of the spectrum. For these reasons, it is not possible to detect broadly distributed ḡ conformations at concentrations of less than 30%. Given the ∼30% total gauche content (ḡ and g combined) in atactic polystyrene,[3] this sensitivity is insufficient.

Conclusions

The backbone torsion angle distribution in PS was investigated by correlating ^{2}H quadrupolar and ^{13}C−^{13}C dipolar NMR interactions, which probe well-defined bond directions. The experimental data show that the maximum in the torsion angle distribution in PS is centered at 180°, within ±10°, and that the trans peak is relatively narrow (<30°). This excludes a recent model with a trans maximum near 200° and with ±30° wide maxima in the torsion angle distribution. While the experiment can in principle identify ḡ conformations based on their distinct line shapes, a combination of various factors prevents the detection of broadly distributed ḡ conformations at concentrations of less than 30%.

Acknowledgment. This work was supported by a Beckman Young Investigator Award and by NSF grant DMR-9703916 to K.S.-R. Support of the NMR facility by NSF/MRSEC is also acknowledged. D.S. gratefully acknowledges financial support from the Wenner-Gren Center Foundation and the Foundation Blanceflor Boncompagni-Ludovisi, nee Bildt.

References and Notes

(1) Tomaselli, M.; Robyr, P.; Meier, B. H.; Grob-Pisano, C.; Ernst, R. R.; Suter, U. W. *Mol. Phys.* **1996**, *89*, 1663.
(2) Schmidt-Rohr, K.; Hu, W. G.; Zumbulyadis, N. *Science* **1998**, *280*, 714.
(3) Dunbar, M. G.; Novak, B. M.; Schmidt-Rohr, K. *Solid State Nucl. Magn. Reson.* **1998**, *12*, 119.
(4) Harris, D.; Bonagamba, T. J.; Schmidt-Rohr, K. *Macromolecules* **1999**, *32*, 6718.
(5) Sandström, D.; Hong, M.; Schmidt-Rohr, K. *Chem. Phys. Lett.* **1999**, *300*, 213.
(6) Schmidt-Rohr, K. *J. Magn. Reson.* **1998**, *131*, 209.
(7) Schmidt, C.; Blumich, B.; Spiess, H. *J. Magn. Reson.* **1988**, *79*, 269.
(8) Schmidt-Rohr, K.; Spiess, H. W. *Multidimensional Solid-State NMR and Polymers*; Academic Press: San Diego, 1994.
(9) Flory, P. J.; Fujiwara, Y. *Macromolecules* **1969**, *2*, 315.
(10) Mattice, W. L.; Suter, U. W. *Conformational Theory of Large Molecules: the rotational isomeric state model in macromolecular systems*; John Wiley & Sons: New York, 1994.
(11) Flory, P. J. *Statistical Mechanics of Chain Molecules*; 2nd ed.; Oxford University Press: New York, 1989.
(12) Spiess, H. W. In *Deuteron NMR− A new tool for studying chain mobility and orientation in polymers*; Spiess, H. W., Ed.; Springer-Verlag: Berlin, 1985; Vol. 66, p 23.
(13) Rapold, R. F.; Suter, U. W.; Theodorou, D. N. *Macromol. Theory Simul.* **1994**, *3*, 19.
(14) Robyr, P.; Muller, M.; Suter, U. W. *Macromolecules* **1999**, *32*, 8681.
(15) Kaji, H.; Schmidt-Rohr, K., to be submitted to *Macromolecules*.
(16) Dunbar, M. G.; Kaji, H.; Azevedo, E. R. d.; Bonagamba, T. J.; Schmidt-Rohr, K., to be submitted to *Macromolecules*.
(17) Khare, R.; Paulaitis, M. E.; Lustig, S. R. *Macromolecules* **1993**, *26*, 7203.

MA992083D